Green Chemistry

Cutting-edge research for a greener sustainable future

Accepted Manuscript

This article can be cited before page numbers have been issued, to do this please use: D. D. van Noordenne, P. Jungbacker, A. Urakawa and F. M. Mulder, *Green Chem.*, 2026, DOI: 10.1039/D5GC06877K.

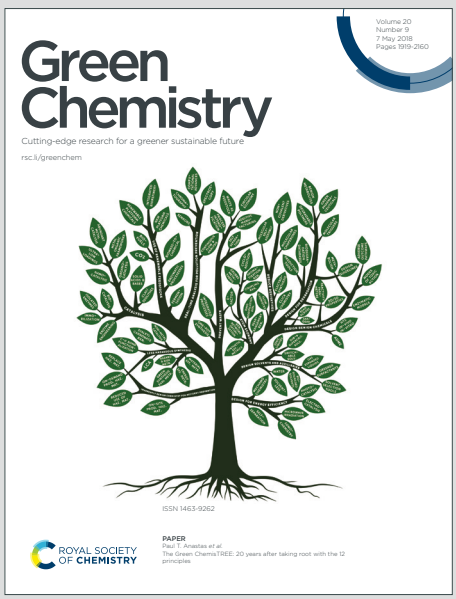

ROYAL SOCIETY OF CHEMISTRY

rsc.li/greenchem

View Article Online
DOI: 10.1039/D5GC06877K

Green Foundation

1. The electrochemical oxidation of ammonia at high selectivity to nitrite and at industrially relevant current densities is presented, with coproduction of green hydrogen for recovery of energy.

2. Nitrogen oxides and salts are used intensively as fertiliser and chemical feedstock, and provide about four times higher value per nitrogen unit than ammonia. When produced using green electrons these materials can be obtained in a green manner.

3. It is shown that high ammonia concentrations in 1M KOH electrolyte can be utilised, going beyond concentrations encountered in wastewater treatment. A cation exchange membrane cell design with $Ni_{0.8}Cu_{0.2}OOH$ as the active catalyst effectively protects the oxidation products from undesirable reduction.

View Article Online
DOI: 10.1039/D5GC06877K

ARTICLE

Electrochemical Ammonia Oxidation at Nickel Copper Hydroxide with H_2 Recovery at High Current Density and Selectivity

Received 00th January 20xx,
Accepted 00th January 20xx

DOI: 10.1039/x0xx00000x

D.D. van Noordenne,[a] P.J. Jungbacker[a], A. Urakawa[a], and F.M. Mulder[a,*]

Electrochemical conversion of ammonia has obtained increasing attention due to the potential applications for fertiliser production and wastewater treatment. This work demonstrates the application of a homogeneously copper-doped nickel hydroxide, prepared through an easily scalable precipitation method, as electrochemical oxidation catalyst. A cation exchange membrane divides the cell and prevents re-reduction of the oxidation product. During chronopotentiometry $Ni_{0.8}Cu_{0.2}(OH)_2$ was able to perform ammonia oxidation, with limited oxygen evolution, from 2.5 mA/cm² up to 400 mA/cm². The Faradaic efficiency for nitrite formation increased with the applied current density. At a high initial ammonia concentration of 1 M, $Ni_{0.8}Cu_{0.2}(OH)_2$ converted 77% of the ammonia in under 3.5 hours, applying a high current density of 400 mA/cm². This resulted in a Faradaic efficiency of 96% total, which is 91% NO_2^- and 5% NO_3^-, which would be impossible in an undivided cell. Therefore, this work demonstrates the potential for efficient and selective ammonia oxidation towards nitrite under industrially-relevant current density and conditions.

Introduction

Humanity relies on the production of synthetic fertilizers to sustain the growing population.[1] In 2021, 187 million tons of ammonia was produced, with 147 million tons for synthetic fertilizer manufacturing. While ammonia is mainly used directly in fertilizer production, a significant amount is converted to nitric acid. This conversion resulted in 67 million tons of nitric acid in 2024.[2] Most of the nitric acid is combined with ammonia to produce synthetic ammonium nitrate fertilizer.

As increasingly renewable energy is implemented, increasing interest exists to produce ammonia and nitric acid electrochemically. Nonetheless, direct electrochemical ammonia production from nitrogen gas and water has yet to reach appreciable and reproducible synthesis rates, compared to the optimized Haber-Bosch process.[3–6] The main challenge is the difficulty of dinitrogen activation, before even being able to optimize the process. However, the subsequent ammonia oxidation to nitrite or nitrate would be more feasible to replace using electrochemistry as one then starts from more electrochemically active ammonia. Currently, large-scale conversion is performed in the multistep Ostwald process, starting with oxidation with O_2 at 10 bar and 800 °C with a Pt/Rh gauze.[7,8] The formed NO is cooled down and reacted with the remaining oxygen to form NO_2. This NO_2 is absorbed with water to form nitric acid. As an alternative in this last step, the application of a hydroxide solution results in nitrite salt rather than the commonly produced nitric acid.[9] In comparison to these process conditions, electrochemistry could make it feasible to produce nitrite and nitrate with more benign conditions and a catalyst consisting of more earth-abundant elements. Furthermore, local application of the product, combined with small-scale ammonia, aligns with the distributed renewable electricity generation. Local production and application could reduce transport costs of both electricity and chemical products. Therefore, it is interesting to investigate the electrochemical ammonia oxidation.

The electrochemical ammonia oxidation reaction (AOR) has been reported for various applications, such as fuel cells and wastewater treatment. [10–18] In these fields, noble metals are commonly applied to achieve high selectivity and conversion to N_2 (Eq. 1). Recent research has shifted focus toward converting ammonia to nitrite (Eq. 2), and nitrate (Eq. 3).[19–22] The oxidation potentials are calculated in the supplementary note 1. Applied conditions, such as concentration, faradaic efficiency (FE) and current density, vary significantly in the literature due to the aim to recover ammonia and nitrate from various wastewater streams (**Error! Reference source not found.**). Nickel is of significant interest as a precious metal free catalyst that can achieve high efficiency and selectivity. Furthermore, nickel is corrosion resistant due to the stability of its solid oxidised species under alkaline and oxidative conditions. The active form is NiOOH, which can either react electrocatalytically (Eq. 4), or result in the indirect oxidation with the reformation of $Ni(OH)_2$ (Eq. 5) and subsequent reoxidation of $Ni(OH)_2$ to NiOOH (Eq. 6).[23] The competing OER reaction and potential above which it can take place is also given (Eq. 7). At the counter electrode, water reduction produces H_2 and OH^- (Eq. 8).

$$NH_{3(aq)} + 3\ OH^- \rightleftharpoons \frac{1}{2}N_2 + 3\ H_2O + 3\ e^- \quad (1)$$
$$E^0 = -0.77\ V\ vs.\ SHE, pH\ 14$$

$$NH_{3(aq)} + 7\ OH^- \rightleftharpoons NO_2^- + 5\ H_2O + 6\ e^- \quad (2)$$
$$E^0 = -0.17\ V\ vs.\ SHE, pH\ 14$$

$$NH_{3(aq)} + 9\ OH^- \rightleftharpoons NO_3^- + 6\ H_2O + 8\ e^- \quad (3)$$
$$E^0 = -0.13\ V\ vs.\ SHE, pH\ 14$$

[a] Chemical Engineering, Faculty of Applied Sciences, Delft University of Technology, 2629 HZ Delft, the Netherlands

$$NiOOH + NH_3 \rightarrow NiOOH + X + n\,H^+ + n\,e^- \quad (4)$$

$$6NiOOH + NH_3 + H_2O + OH^- \rightarrow 6Ni(OH)_2 + NO_2^- \quad (5)$$

$$Ni(OH)_2 + OH^- \rightleftharpoons NiOOH + H_2O + e^- \quad (6)$$

$$E^0 = 0.49\ V\ Vs\ SHE, pH\ 14$$

$$4OH^- \rightleftharpoons O_2 + 2H_2O + 4e^- \quad (7)$$

$$E^0 = +0.40\ Vs\ SHE, pH\ 14$$

$$2\,H_2O + 2e^- \rightleftharpoons H_2 + 2\,OH^- \quad (8)$$

$$E^0 = \text{-}0.83\ Vs\ SHE, pH\ 14$$

The layered nickel hydroxide structures have been doped with various metals to improve their properties.[19,21,24–26] The most promising approach is the addition of copper to the nickel hydroxide, resulting in a catalyst highly active for ammonia oxidation. For example, Jiang *et al.* reported selectivity up to 99% towards nitrite for wastewater denitrification relevant conditions of 1 mM NH_3 and 0.1 M KOH electrolyte.[20] However, they presented and analysed a nanostructured phase separated catalyst material of $Ni(OH)_2$ and $Cu(OH)_2$. Possibly at the interface of these materials there could be the activity enhancing phase compared to the two pure phases.

In our research we found that it is possible to produce a homogeneous Cu doped $Ni_{1-x}Cu_x(OH)_2$ phase. Compared to the heterogenous mixture, one may expect that now all the material has influence of the Cu doping and it could thus result in improved activity with respect to pure and inhomogeneously Cu doped $Ni(OH)_2$ catalyst. Here, we report the application of a homogenously copper-doped nickel hydroxide electrode, $Ni_{0.8}Cu_{0.2}(OH)_2$.

Figure 1. The difference between performing the AOR in alkaline electrolyte within a) an undivided cell and b) a cell divided with a cation exchange membrane. The ionic current can be carried by K^+, while the product anions NO_2^- are blocked. NH_3 in the feed can only react at the positive electrode. At the alkaline pH ammonia remains NH_3(Aq).

Besides catalyst, the experimental cell can significantly influence the achieved results with AOR, commonly performed in a single cell compartment. In such a configuration the formed nitrite and nitrate anions remain dissolved in the electrolyte and are reducible at the counter electrode to NH_3 and N_2 (**Error! Reference source not found.**a). To prevent this, it will be shown that a cation exchange membrane (CEM) should be applied to prevent such anion crossover and re-reduction of the oxidation products (**Error! Reference source not found.**b). Within this study, we shall establish the advantage of applying a divided CEM cell for AOR compared to an undivided cell and also show the high conversion and current densities that can be reached with the homogeneous $Ni_{0.8}Cu_{0.2}(OH)_2$ catalyst. The CEM appears crucial to achieve high product selectivity and FE and to determine the FE unambiguously. Furthermore, we show that it becomes possible to work with concentrated ammonia solutions as well as current densities up to 400 mA/cm^2.

Experimental

All chemicals were obtained from Sigma Aldrich and were used as purchased. All water mentioned is Mili-Q water with a conductivity of <0.1 µS/cm. A 28 wt.% NH_3 concentrated solution was used. A high concentration solution of ammonia in 1 M KOH was prepared by slowly mixing the appropriate KOH solution and 28 wt.% NH_3. The resulting solution was kept in a closed container to limit ammonia losses.

Synthetic procedures

To obtain a homogeneously mixed Ni-Cu phase material, a previously reported co-precipitation method was applied and modified for addition of Cu instead of Fe.[27] An aqueous solution containing $NiSO_4 \cdot 6H_2O$ (0.25 M, 50 mL, 20.6% Ni) with corresponding amount of $CuSO_4$ (0.0625 M, 99%) was prepared to obtain the $Ni_{0.8}Cu_{0.2}(OH)_2$ material. Under vigorous stirring of the KOH (2.0 M, 100 mL) solution, the metal precursor solution was added dropwise. The precipitate was collected by centrifuge (3500 rpm, 10 min), and after washing twice with water and once with ethanol. The residue was dried at 50 °C under vacuum. Ball milling at 200 rpm for 15 min resulted in the powdered material for preparing the electrodes.

Material Characterisation

X-ray diffraction was performed using a Bruker D8 Advance ECO diffractometer equipped with a Cu-K_α source ($K_{\alpha1}$=1.54060 Å, 40 kV and 25 mA) and Lynxeye-XE-T position sensitive detector. Fixed divergence slit was applied with a Bragg-Brentano geometry. A step size of 0.02° with a measuring time of 0.1 s/step was employed. SEM and EDS were performed on both the powders and used electrodes using a SEM-JEOL-6010LA.

Electrode Preparation

Electrodes were prepared through homogenously mixing the material ($Ni_{1-x}Cu_x(OH)_2$) with 50 wt.% carbon super P® and 50 wt.%

graphite through pestling. The binder polyethersulfone (7 wt.% in N-methylpyrrolidon) was added to obtain a slurry. The nickel foam matrices (0.5 mm thick, 99.9% Ni) were prepared by cutting 20×20 mm squares. These squares were cleaned in HCl (4 wt.%) and acetone for 5 min each in a sonication bath. After pasting, the slurry was solidified through phase inversion in water.[28,29] Such electrode processing method is known to result in highly porous electrodes with large electrochemical surface area, i.e. which is advantageous for relatively high current densities. The electrodes were dried under vacuum at 50 °C.

Electrochemical experiments

Cyclic voltammetry was performed with a Parstat MC-1000 system with a three-electrode setup. The Tafel slope and chronopotentiometric measurements were executed on a Maccor 4000 battery cycling system. These were mainly performed in a three-electrode setup. Auxiliary potential channels could be connected to measure cell potential and the potential of counter electrode in comparison to a second Hg/HgO reference electrode.

Cyclic voltammetry and measurements without membranes were performed in a single compartment cell with nickel foam counter electrode and Hg/HgO (KOH) reference electrode. Experiments with a membrane were performed with a 20 mm diameter Nafion 117 membrane in between two 50 mL electrolyte compartments. If ammonia was added, it was added on both sides of the membrane to reduce the effect of initial differences in ammonia concentration and pH on the measurements, and to demonstrate the limited poisoning effect of ammonia on the counter electrode. Before performing ammonia oxidation during chronopotentiometry, the cell was operated at the same current density without ammonia until a stable potential was achieved. This was to stabilize the electrode in the nickel oxyhydroxide state and convert all potential nitrogen contamination[30] to nitrogen gas, nitrite, and nitrate to improve accuracy.

Cyclic voltammetry was performed in 1 M KOH in the range of 0–0.63 V vs. Hg/HgO at a scan rate of 1 mV/s. This was followed with the addition of 50 mM NH_4OH and repeated. The fifth cycle was used for analysis. The Tafel slope measurements were performed by initially applying a current to convert all hydroxide in the catalytic material into oxyhydroxide before applying constant current for 10 min at increasing current densities. A range from 0.25 mA/cm^2 up to 25 mA/cm^2 was applied, where the area refers to the geometric surface area.

Ion Chromatography

The concentration of anions in the electrode were determined with the use of an ion chromatograph (IC). The system consisted of an Thermo Scientific™, Dionex™ Integrion™ HPIC™ System equipped with a conductivity detector and an AS18-Fast anion column. In accordance with Thermo Scientific application note 72481, AutoNeutralization™ was applied to improve accuracy by removing the KOH background without dilution. A gradient in the KOH concentration of the eluent was applied to obtain completely separated nitrite and nitrate peaks for maximal accuracy.

Results & Discussion

X-ray diffraction (XRD) was applied to confirm the formation of $Ni_{0.8}Cu_{0.2}(OH)_2$, denoted as $NiCu_{0.2}$, synthesized through a precipitation method under alkaline conditions. The same synthesis method was applied with the individual nickel and copper salt, which clearly formed two distinguishable materials (Figure 2). The nickel precipitated as β-$Ni(OH)_2$ phase, consistent with the reference pattern. The copper salt formed CuO, as $Cu(OH)_2$ can lose water during drying. The XRD pattern of $NiCu_{0.2}$ indicates the formation of β-$Ni(OH)_2$ with a potentially minimal peak shift, indicating successful doping of the copper. The absence of a separated phase suggests that the Cu is homogenously incorporated.

Figure 2. XRD pattern of $NiCu_{0.2}(OH)_2$ in comparison to β-$Ni(OH)_2$ and

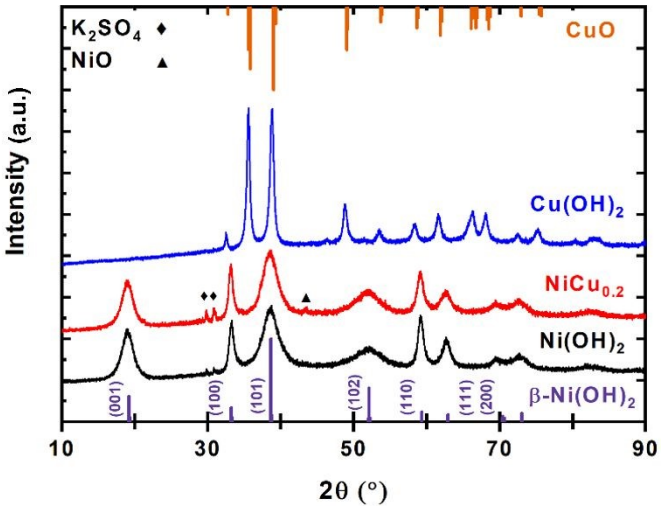

$Cu(OH)_2$ made through the same synthesis method. At the bottom a β-$Ni(OH)_2$ (COD 1011134) reference pattern and at the top a CuO (COD 1011148) reference pattern are shown. The $NiCu_{0.2}(OH)_2$ is closely resembling the β-$Ni(OH)_2$.

Further confirmation of homogenous incorporation of the copper was done with SEM and EDS (Figure 3). The $NiCu_{0.2}$ particles consist of crystallites but the presence of a background indicates also amorphous material in between. EDS analysis shows a homogenous distribution of Ni and Cu, suggesting copper is homogenously incorporated in the $Ni(OH)_2$. Furthermore, a Ni:Cu ratio of 0.83:0.17 throughout the powder was determined. This is close to the theoretical ratio. Potassium and sulphate are present as crystalline K_2SO_4 contaminant from the precipitation method. This salt was further washed out during the electrode preparation (**Error! Reference source not found.**). Overall, these results demonstrate homogenously incorporated copper to form $NiCu_{0.2}$.

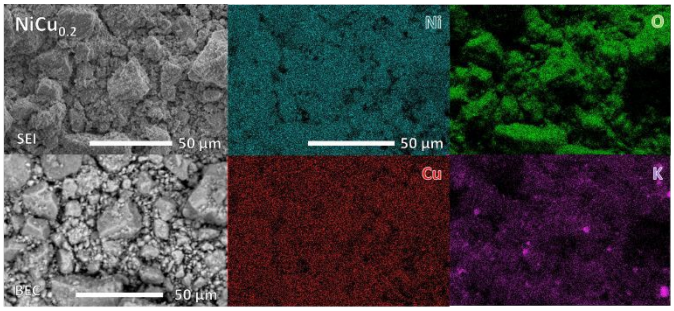

Figure 3. SEM and EDS images of $NiCu_{0.2}$ with separate images indicating the presence of Ni, Cu, O and K. K inhomogeneous distribution correlates with sulphur and originates from separated

K_2SO_4 salt from the precipitation synthesis method. Both secondary electron imaging (SEI) and backscatter electron imaging (BEC) modes of SEM are applied to show topography and composition, respectively.

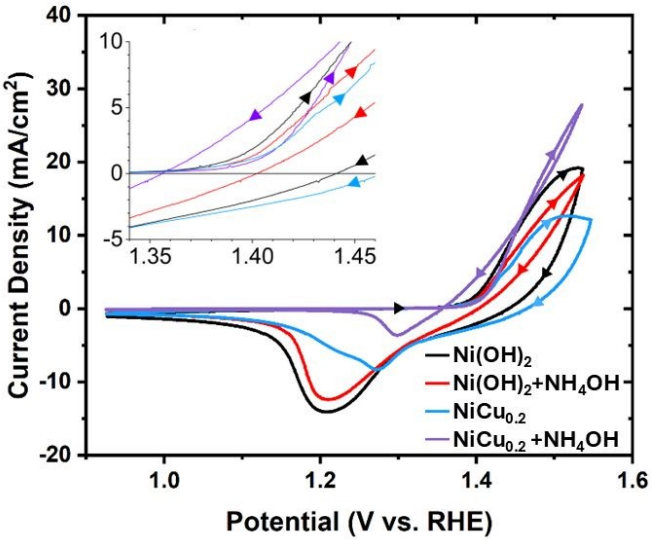

Figure 4. Cyclic voltammetry of $Ni(OH)_2$ and $NiCu_{0.2}$ in 1 M KOH with and without 50 mM NH_4OH. A scan rate of 1 mV/s was used. Current densities refer to the geometric surface area.

Cyclic voltammetry was applied to investigate the catalyst and its AOR activity (Figure 4). The $Ni(OH)_2$ reference exhibits two redox peaks. The anodic peak is the overlapping Ni^{2+}/Ni^{3+} oxidation peak and the OER activity, with an onset potential of 1.39 V vs. RHE. The reduction peak originates from the reduction of both γ-NiOOH to α-$Ni(OH)_2$ and β-NiOOH to β-$Ni(OH)_2$, with the γ-NiOOH reduction occurring at a more positive potential.[31] In general γ-NiOOH is associated with higher attainable Ni^{3+} to Ni^{4+} valences which are charge compensated by anion and water incorporation in the layered structure. The incorporation of Cu has resulted in limited change in onset potential of the oxidation peak, but the current density was significantly reduced. Also in the Tafel plots in Figure 5 it can be observed that the $NiCu_{0.2}$ has lower OER at the same applied potential. This lower OER activity is beneficial to suppress the competing OER and can therefore increase AOR FE. The cathodic peak shape is different from pure $Ni(OH)_2$, which seems to be related to more γ-$NiCu_{0.2}OOH$ reduction at more positive reduction potential, compared to less β-$NiCu_{0.2}OOH$ reduction. This suggests that significant phase conversion to γ-$NiCu_{0.2}OOH$ occurs during oxidation.

The addition of ammonia to the electrolyte resulted in a 10 mV reduction of onset potential for oxidation with β-$Ni(OH)_2$. However, the overall peak current density decreased, suggesting that $Ni(OH)_2$ has a limited AOR activity. The smaller reduction peak implies that AOR occurs, as less current is available for NiOOH formation. In contrast to $Ni(OH)_2$, $NiCu_{0.2}$ has an increased oxidation current density with significant peak shape change in the presence of ammonia. Initially, the cathodic scan has a similar current density to the anodic scan, before surpassing it as it drops to zero at 1.35 V vs. RHE. This enhanced activity originates from AOR on the oxyhydroxide formed during oxidation, and continues with indirect AOR below the onset potential of the anodic scan, reforming oxyhydroxide back to hydroxide (Eq. 5). The smaller $NiCu_{0.02}OOH$ reduction peak with ammonia present confirms this mechanism. These results indicate that AOR is limited by the formation of NiOOH from $Ni(OH)_2$. The onset potential of AOR is therefore equal to the potential of NiOOH formation.[20] The higher AOR activity would then be an intrinsic property of $NiCu_{0.2}$, which can be related to Cu with its valence limited to 2+ affecting the Ni^{2+}:Ni^{3+}:Ni^{4+} ratio and the $NiCu_{0.2}(OH)_2$ and β- and γ-$NiCu_{0.2}OOH$ or mixed 'interstratified' phase formation.[20,24,32–36] The remaining cathodic peak is also at the more positive potential side, associated rather with γ-$NiCu_{0.2}OOH$ reduction to α-$NiCu_{0.2}(OH)_2$ than with β-$NiCu_{0.2}OOH$. That may indicate that especially the β-$NiCu_{0.2}OOH$ is active in the (indirect) AOR as the β-phase is apparently already reduced following equation (5) before the cathodic sweep reaches down to its reduction potential in absence of NH_3. To elucidate the reaction mechanism is challenging and may require in-operando XRD and EXAFS characterisation methods during AOR to provide insight in the phase behaviour and state of Ni and Cu[18], while in operando near ambient pressure XPS could potentially observe relevant N species. [37]

Tafel plots were measured to further investigate the difference in the reaction kinetics between $Ni(OH)_2$ and $NiCu_{0.2}$. They were measured with an initial anodic current to convert all hydroxide material to oxyhydroxide, because NiOOH is the AOR active material. In the Tafel plot, a low and high overpotential range is observed (Figure 5). At low current densities, the Tafel slopes are 43 and 72 mV/dec for $Ni(OH)_2$ and $NiCu_{0.2}$, respectively. The difference is more significant in the high overpotential range, with 96 and 169 mV/dec, respectively. These higher Tafel slopes indicate a lower OER activity for $NiCu_{0.2}$, which should limit OER activity during ammonia oxidation, increasing the FE.

The addition of ammonia results in significant changes in both Tafel slope and potential. At 10 mA/cm^2 we found a reduction of potential from 0.624 to 0.465 V and 0.662 to 0.469 V vs. Hg/HgO for $Ni(OH)_2$ and $NiCu_{0.2}$, respectively. For $Ni(OH)_2$, this coincided with a Tafel slope increase to 62 mV/dec. In the high overpotential range, the Tafel slope changes to 186 mV/dec. The significant increase in slopes indicates sluggish AOR activity with intermediate coverage limiting the OER. In comparison, the Tafel slopes of $NiCu_{0.2}$ reduce to 49 and 140 mV/dec for the low and high current density range, respectively. This explains the higher AOR activity measured with cyclic voltammetry. With this reduction in Tafel slope, it can be expected that at high current densities $NiCu_{0.2}$ would be able to maintain high AOR selectivity. This as a result of OER activity being limited by the higher onset potential and Tafel slope. Therefore, we will focus on $NiCu_{0.2}$ to evaluate the effect of experimental conditions and cell layout on the ammonia oxidation.

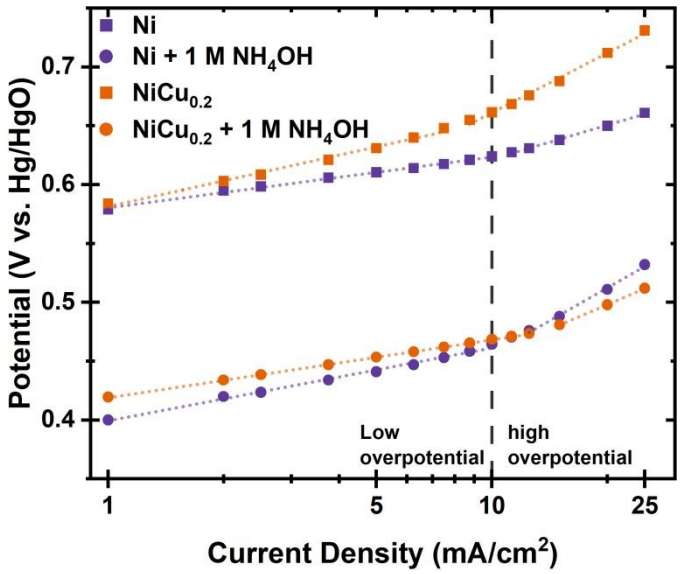

Figure 5. The Tafel plot of $Ni(OH)_2$ and $NiCu_{0.2}$ for OER and AOR in 1 M KOH with and without 1 M dissolved NH_3 based on stepwise increase of current density to reduce error caused by gas bubble formation. Dashed line added to illustrate the divide between low and high overpotential range.

Electrolyte and pH Dependence of The Ammonia Oxidation Reaction

High AOR activity has been exhibited by $NiCu_{0.2}$. Nonetheless, the supporting electrolyte and ammonia concentration can significantly influence the AOR selectivity and FE. Therefore, understanding the effect of electrolyte is crucial to achieve high FE and selectivity under industrial relevant conditions. The influence of the electrolyte was investigated in a single compartment cell (**Error! Reference source not found.**a) to establish the impact of electrolyte composition and undivided cell. Each experiment was started with achieving a stable potential without ammonia present to form the active NiOOH material, before initiating the experiment with the addition of dissolved ammonia. This method removes apparent FE losses that are solely related to $Ni(OH)_2$ oxidation to NiOOH, and representing a continuous industrial ammonia electrooxidation process. The nitrite and nitrate production was monitored while the latter concentration was negligible and is therefore omitted for clarity, unless relevant for discussion.

The application of 1 M NH_4OH as the electrolytes resulted in a FE of 34% for conversion of ammonia to nitrite in the initial 4 hours, with consistent nitrite formation (Figure 6). However, after 22 hours, the nitrite concentration decreased. This agrees with our earlier statement of the unobstructed access to the counter electrode resulting in reduction of nitrite, achieving an equilibrium concentration. In comparison, concentrated ammonia (28 wt.%, 14.5 M) reduced the nitrite formation rate and a FE of 10% for the initial 4 hours was determined. After 22 hours, only a slight increase in nitrite concentration is measured, implying that the additional ammonia does not promote the reaction. Furthermore, a pH effect was observed. Medvedev *et al.* reported that $Ni(OH)_2$ switch to producing nitrate below pH 12.[38] This is near the pH of the electrolyte with 11.6 and 12.2 respectively for 1 M and 14.5 M NH_4OH. The pH is further lowered with the conversion of the basic ammonia to the strong acids nitrous and nitric acid. This is confirmed with an increase in nitrate to 0.16 and 0.29 mM after 22 hours for 1 M and 14.5 M ammonia, respectively.

The results indicate that the addition of alkaline supporting electrolyte, KOH, is required to stabilize the pH. The addition of 1 M KOH to 14.5 M NH_4OH electrolyte resulted in no notable difference within the initial 4 hours. Despite this, after 22 hours a higher nitrite concentration was established. In comparison, 1M KOH and 1M NH_4OH combined had a significantly higher initial production rate, without noticeable end concentration difference. The initial rate would mainly depend on direct catalytic effect, suggesting that ammonia or reaction intermediates block active sites with 14.5 M NH_4OH, limiting the rate. The addition of 1 M KOH to 1M NH_4OH promoted AOR, suggesting that the higher pH is not detrimental to AOR, rather an optimal ammonia concentration between 1 and 14.5 M exists. The similar higher end concentration originates from the OH^- ion conductivity, reducing the transport number of nitrite and the correlated nitrite mobility and its (detrimental, nitrite loss making) reduction at the counter electrode. The KOH concentration was further increased to 6 M KOH with 1 M NH_4OH to investigate if this can enhance nitrite production. However, the nitrite formation rate decreased, likely due to the reduced NH_3 solubility and increased vapor pressure with higher KOH concentration.[39] As a result, less NH_3 is available for oxidation within the electrolyte. The production rate was still linear for 4 hours, confirming that FE loss does not originate from NH_3 loss over time. Therefore, we chose to continue with 1 M KOH with 1 M NH_4OH for the following experiments, as it should result in the highest FE and stability (Figure 7).

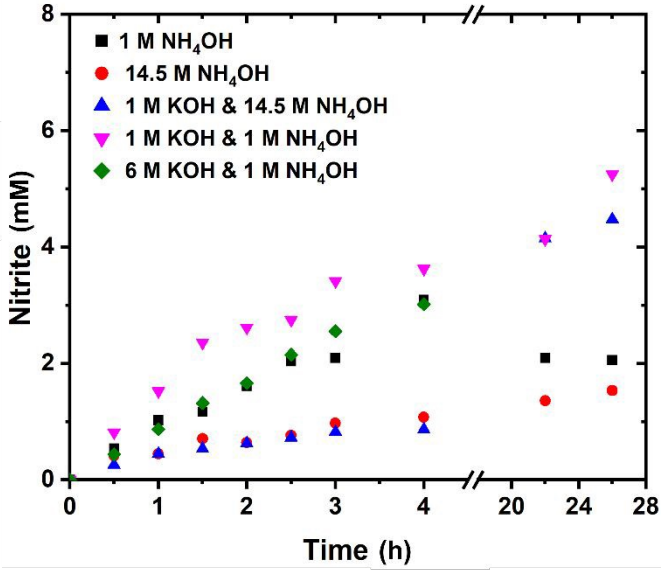

Figure 6. Bulk electrochemical oxidation of ammonia under various conditions at 5 mA/cm² with $NiCu_{0.2}$ as the catalyst. Only the nitrite concentration is shown as the nitrate concentration was negligible unless otherwise mentioned.

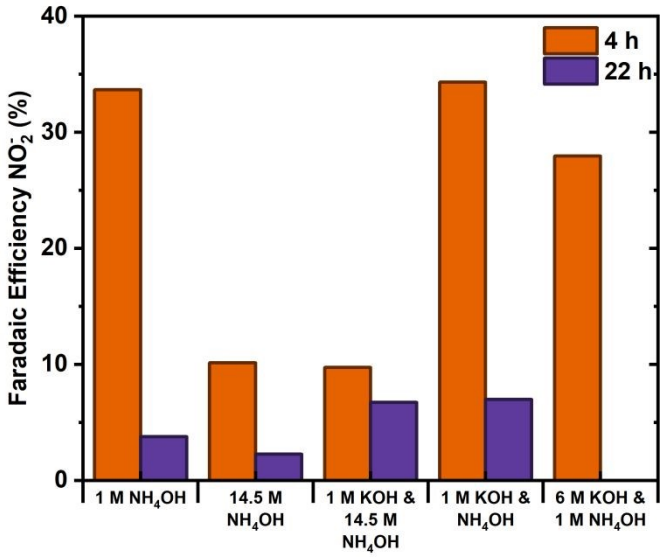

Figure 7. Summary of the Faradaic efficiency towards nitrite for the initial 4 hours and the total 22 hours of the abovementioned experiment within a single compartment cell with $NiCu_{0.2}$ at 5 mA/cm^2.

Cation Membrane Integration for Increased Yield and Product Separation

The 1 M KOH limits the experimental runtime due to the change in pH. Therefore, the experiment was repeated with 6 M KOH to determine if prolonged conversion could be achievable. Furthermore, the cell was reduced from 125 to 50 mL for each compartment to improve performance. This reduction decreased the electrode gap, measuring time and ammonia vapour losses. Vapour loss was further reduced by limiting air contact through further sealing. The experiments were terminated when the initial OER potential, established before ammonia addition, was reached. This result in an insignificant ammonia concentration remaining, while preventing electrode damage from reduced pH.

An H-cell divided by a Nafion 117 CEM is chosen as setup for preventing reduction of nitrite and nitrate at the counter electrode, as this has very limited nitrite and nitrate anion transport and high cation transport. In this case K^+ transport is dominant as it has a high concentration at 1M KOH and protons are essentially absent. Ammonia was added to both sides of the membrane to mitigate ammonia crossover. The initial results achieved with this setup in 1 M KOH with 1 M NH_3 electrolyte at 10 mA/cm^2 are promising with a constant production of nitrite for 70 hours (Figure **8**a). This is a significantly longer runtime with constant production, resulting in a yield of 150 mM nitrite, demonstrating the detrimental effect of product reduction at the cathode in absence of the membrane. After these initial 70 hours, the nitrate concentration increases exponentially, due to the depletion of OH^- and reduction in pH to below 9. This coincided with an increase in potential due to the reduction of conductivity from the lower electrolyte concentration (Figure **8**b). The change in pH and depletion of OH^- is expected under alkaline conditions, because the CEM transfers K^+ through the membrane, while simultaneously OH^- is consumed within the anolyte. NH_4^+ could also be transported as cation, however, at the applied pH its presence is suppressed in favour of neutral dissolved NH_3. The pH dependence of nitrite oxidation to nitrate was confirmed by performing an experiment in 1 M KOH with 1 M KNO_2 (**Error! Reference source not found.**). Only 33 mM nitrate was formed after 6 hours. When the measured oxidation potential has significantly increased, indicating the lowering of pH, almost complete conversion to nitrate was obtained. Therefore, maintaining a stable alkaline pH is crucial to achieve high nitrite selectivity.

The initial results with 6 M KOH in the electrolyte were obtained with a total operation time of 76 hours with minimal nitrate formation (**Error! Reference source not found.**). A lower FE of 52% at 2.5 mA/cm^2 towards nitrite was obtained, in comparison to 97% for the previous measurement with

1 M KOH at 10 mA/cm^2. The limited activity in 6 M KOH could originate from the limited formation rate of $NiCu_{0.2}OOH$ due to the lower potential at the applied current density. The reaction was initiated with a potential of 0.33 V vs. Hg/HgO. This is just above the $NiCu_{0.2}(OH)_2/NiCu_{0.2}OOH$ equilibrium potential for $NiCu_{0.2}(OH)_2$ at a low state of charge, indicating a $NiCu_{0.2}OOH$ surface could be formed.[27,40,41] Also when comparing the experiment with a pure $Ni(OH)_2$ electrode (**Error! Reference source not found.**) the Cu doped sample does directly show a higher potential but rather a lower rate as the AOR seems to be potential dependent. In combination with the CV scans in Figure

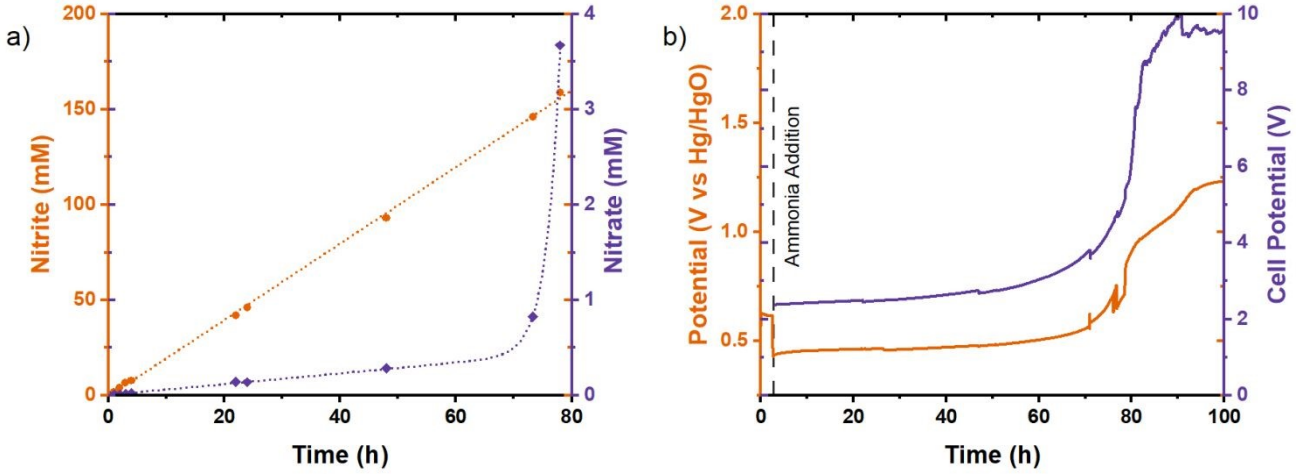

Figure 8. Chronopotentiometry of $NiCu_{0.2}$ electrode performing AOR in 1 M NH_3 in 1 M KOH at 10 mA/cm^2 in glass H-cell divided by Nafion

117 cation exchange membrane. a) concentration of products during chronopotentiometry and b) the measured potentials. Left graph stops at 80 hours, as the results of the last 20 hours were not representative.

View Article Online
DOI: 10.1039/D5GC06877K

Figure **4**, we conclude that the current and resulting potential are too much on the onset of AOR activity, while the increased AOR activity requires higher potentials. In addition, Figure 5 shows the potential at the same low current density of the $NiCu_{0.2}$ sample to be higher

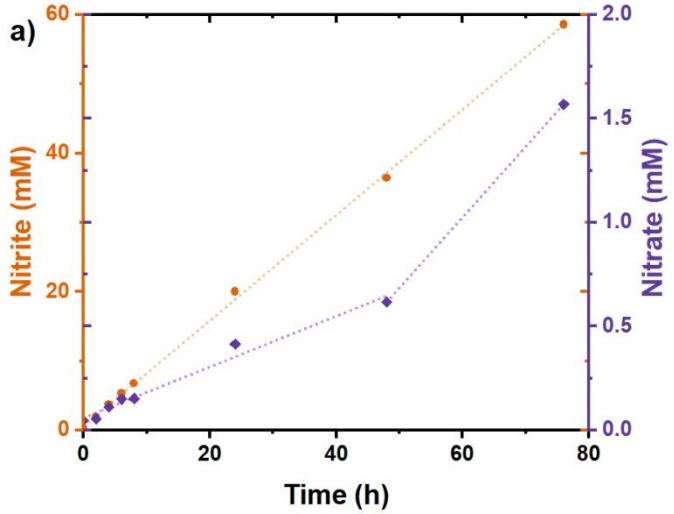

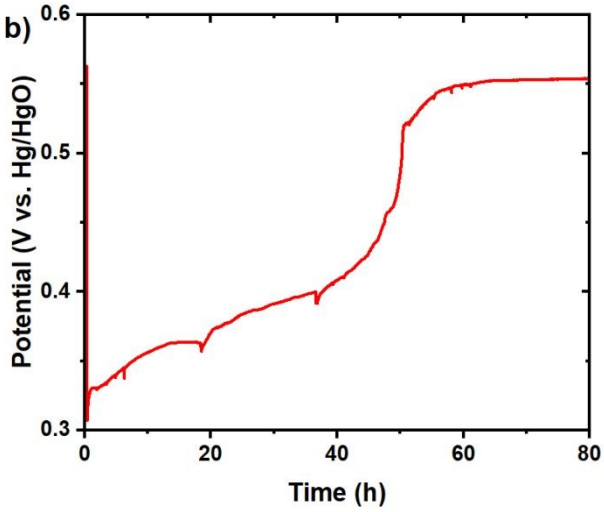

than for pure Ni, which would bring it closer to OER. Thus, increasing the current density and the correlated potential should increase the $NiCu_{0.2}OOH$ formation rate and subsequent AOR to nitrite, and move into the current and potential territory where the $NiCu_{0.2}$ in the presence of ammonia requires a lower potential for the same current. Therefore, to promote the AOR, the current density was raised to 25 mA/cm^2 (Figure 10). and 1 M KOH was compared with 6 M KOH again. The 1 M KOH electrolyte had a limited runtime of 14 hours with a higher potential in comparison to 6 M KOH (Figure 10b). Furthermore, the potential with 6 M KOH electrolyte was significantly lower than expected based on the pH difference (Figure 10c). It is expected to originate from the AOR and will result in improved energy efficiency. In the initial 8 hours, nitrite FE was 87% for 1 M KOH, slightly higher compared to 82% for 6 M KOH. However, the difference in FE is less significant than the potential reduction. The addition of ammonia resulted in a potential drop of 0.20 V with 1 M KOH, compared to 0.24 V with 6 M KOH. This effect was further demonstrated by the cell potential. The addition of ammonia reduced the potential to 2.67 V from 2.76 V with 1 M KOH. Whereas a 12% reduction from 2.24 V to 2.08 V was recorded with 6 M KOH. These potentials are higher than the theoretical potential due to activation overpotentials, and the electrode gap and its resulting significant internal resistance. Furthermore, the prolonged stable activity with 6 M KOH resulted in 49% conversion after 48 hours with 78 and 4% FE towards nitrite and nitrate, respectively. These promising results invited further increasing the current density as that could result in even higher FE as we approach industrial relevant current density.

View Article Online
DOI: 10.1039/D5GC06877K

ARTICLE

Figure 9. Chronopotentiometry of $NiCu_{0.2}$ in 6 M KOH with 1 M NH_3 at 2.5 mA/cm². a) measured nitrite and nitrate concentration with dashed lines for linear trend lines. b) shows the measured potential during the chronopotentiometry.

Figure 10. Product concentration for chronopotentiometry with $NiCu_{0.2}$ at 25 mA/cm² in the cation membrane divided cell a) 1 M KOH with 1 M NH_3 and b) 6 M KOH with 1 M NH_3. c) potential measured during the chronopotentiometry. d) absolute potentials measured during the chronopotentiometric measurement for first hour of the 6 M KOH with 1 M NH_3. Ammonia addition illustrated with dashed line. Working electrode (red) and counter electrode (black) were measured against their own reference electrode. Cell potential is marked green.

To further prove the feasibility of industrial electrochemical ammonia oxidation, the current density was increased to 400 mA/cm². Within less than 3,5 hours, 769 mM of ammonia was converted to nitrite and nitrate (Figure 11a). The initial OER potential of 0.80 V vs. Hg/HgO reduced to an AOR potential of 0.60 V vs. Hg/HgO upon ammonia addition (Figure 11c). The limited potential decrease of 20 mV from the counter electrode, suggests minimal poisoning effect on hydrogen evolution. A total cell potential of 2.0 V was calculated, ignoring internal resistances. The theoretical equilibrium cell potential should be 1.3 V, the difference between Eq. 6 and 8, as (2) only occurs when the NiOOH is present. A significant difference originates from the non-optimised counter electrode and the high overpotential. Further cell optimisation outside this study is required to actually reach reduced potentials closer to the equilibrium potential. At the higher applied current density and potentials a nitrite FE of 91% and total FE of 95% were achieved (Figure 11b). Meanwhile, the potential exceeds the onset potential of OER, but did not result in significant OER activity. Ammonia and AOR intermediates limit O_2 formation while enhancing nitrite formation. This is either occurring by occupying actives sides with intermediates and ammonia, or reacting with the OER intermediates.[42] OER requires the formation of NiOOH, which is rapidly consumed through indirect AOR when locally present. This agrees with the lower AOR Tafel slope of $NiCu_{0.2}$, indicating higher activity for AOR than OER.

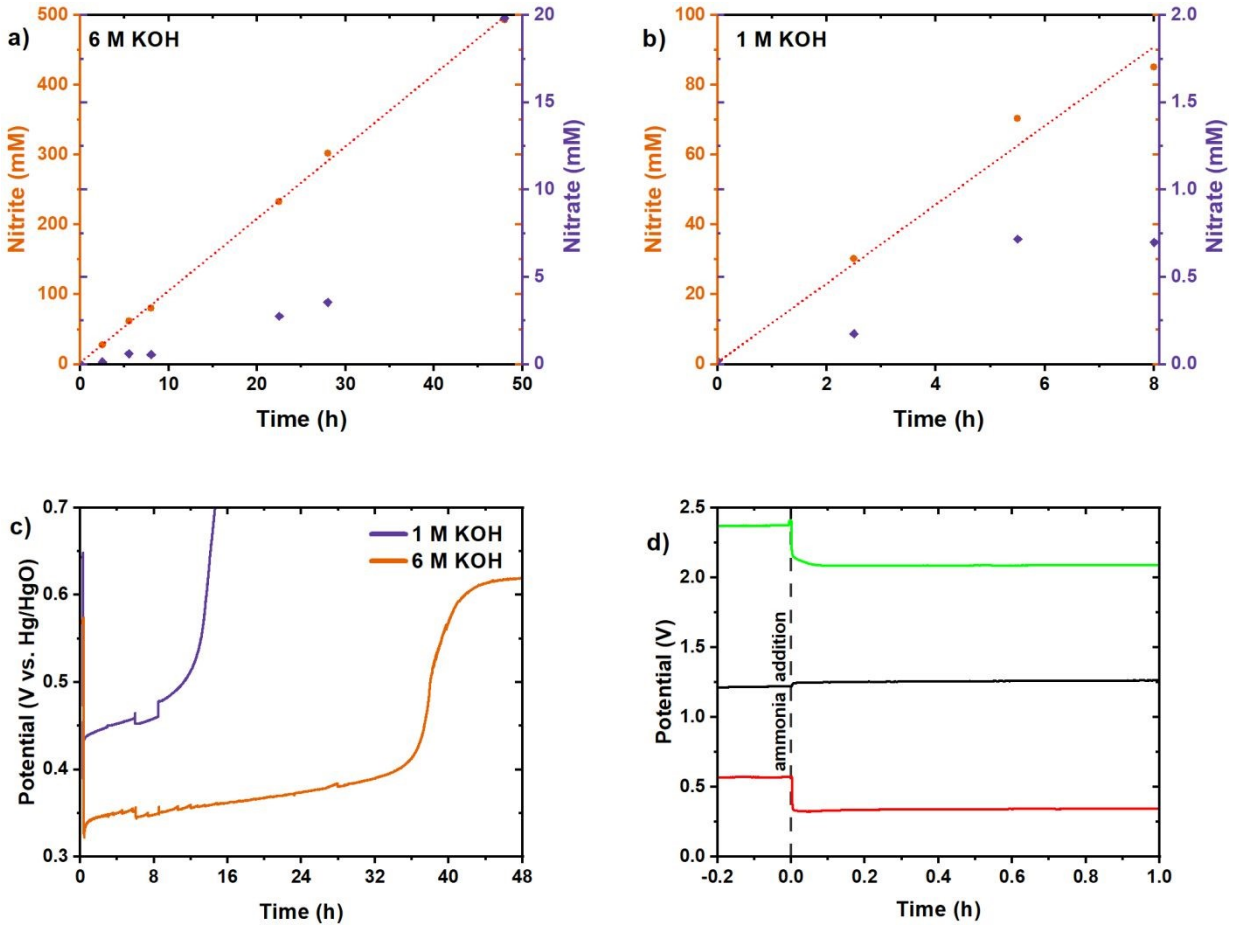

View Article Online
DOI: 10.1039/D5GC06877K

ARTICLE

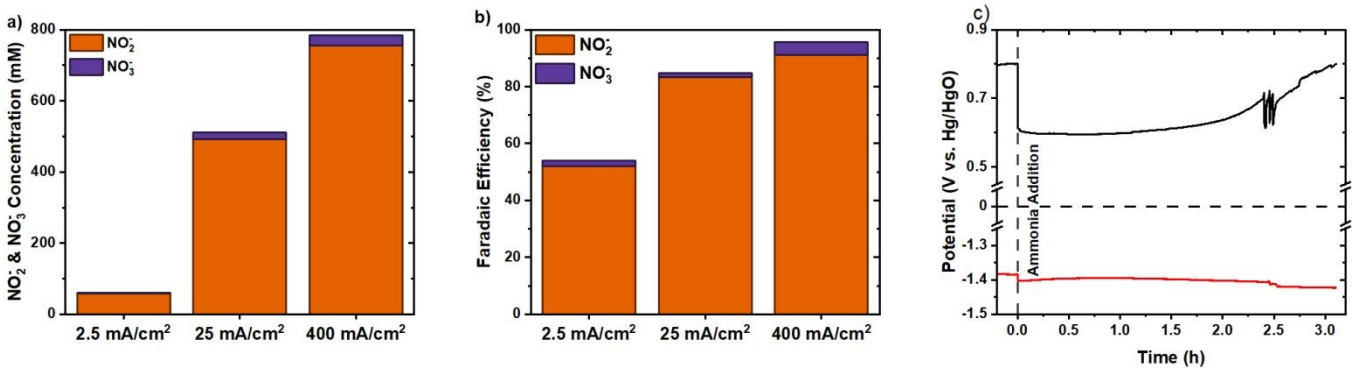

Figure 11. AOR in cation membrane divided cell. a) Nitrite and nitrate concentration for the chronopotentiometric measurement with $NiCu_{0.2}$, at the end of the measured within 6 M KOH with 1 M NH_3 at various current densities. b) summary of the Faradaic efficiency achieved for the chronopotentiometric methods under increasing current density. c) measured potential at a current density of 400 mA/cm² for working electrode (black) and counter electrode (red) against their own reference electrode in their compartment.

Comparison with previous results

As stated in the introduction, comparison with literature for AOR catalysts is in Table S1. The AOR towards nitrite and nitrate is reported mostly for Cu and Ni or Co based catalysts, while noble metal based catalysts mostly yield N_2. The yields of nitrate and nitrite yield a maximum FE of above 86% for current densities applied of 2 mA/cm². The maximum current densities applied ~100 mA/cm² yield about 5% FE conversion to nitrite. The presently observed 400 mA/cm2 and FE of 96% therefore advances the AOR significantly towards industrially relevant values.

Direct comparison is difficult because the Ni-Cu based materials are reported to be inhomogeneous mixtures of $Ni(OH)_2$ and $Cu(OH)_2$, or Cu-Ni metal alloys. The latter will have an oxidised (oxy-)hydroxide surface since the potentials applied are well above their oxidation potentials. Also note that their AOR potentials are above OER/ORR vs. RHE eq. 7, and therefore more positive than the equilibrium potentials of eq. 1, 2 and 3, excluding spontaneous fuel cell operation. The published onset potential changes in a representative example by Xu *et al.* are small when comparing in situ grown inhomogeneously mixed $Ni(OH)_2$ and $Cu(OH)_2$ based nanowires with and without ammonia.[24] This is also the case for the $Ni(OH)_2$ and $NiCu_{0.2}$ reported here as the oxyhydroxide formation is determining the onset potential. In addition, the Tafel slopes with 55 mM NH_4^+ concentration are similar as we observe in 1 M NH_3. However, in [24] the current density saturated above a concentration of 150 mM, which will mean lower currents in the Tafel experiment at higher concentrations. The reported oxidation product at their attainable 9 mA/cm² after 24h is about 19% FE nitrate, while now with the homogeneously prepared $NiCu_{0.2}$ we report below constant current densities up to 400 mA/cm² and high FE conversion to nitrite. Also pure $Ni(OH)_2$ is reported in membrane separated cells to reach promising AOR activities at up to ~30 mA/cm², with 0.2 M NH_4OH, but with still significant N_2 production (20-90% FE) next to nitrite and nitrate yields that depend on pH. OER will make up the missing current amounts at the applied potentials.

Electrode Stability

Long-term stability of the electrode material is fundamental to ensure cost-effective industrial application. The XRD pattern of the used electrode is comparable to the original powder, with the β-$Ni(OH)_2$ phase as the main contributor (Figure 12). Additional peaks correspond to the nickel foam, graphitic carbon, $KOH \cdot 2H_2O$ and $KHCO_3$. Furthermore, no separated copper oxide or peak shift were detected, indicating a limited change within the crystalline material.

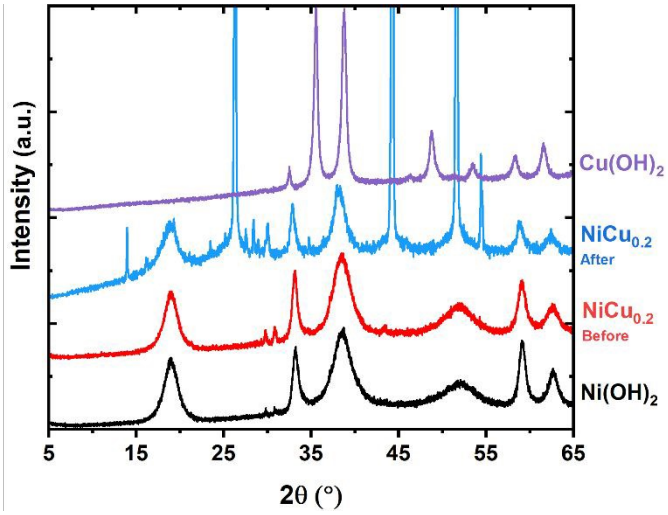

Figure 12. XRD pattern of $NiCu_{0.2}$ used for the experiment with 6 M KOH and 1 M NH_3 at 400 mA/cm^2 for close to 3.5 hours. $Ni(OH)_2$ and $Cu(OH)_2$ powder added as reference for related peaks. The four biggest sharp peaks originate from graphitic carbon and nickel present in the electrode. $NiCu_{0.2}$ powder added for comparison of the phase and potential peak change.

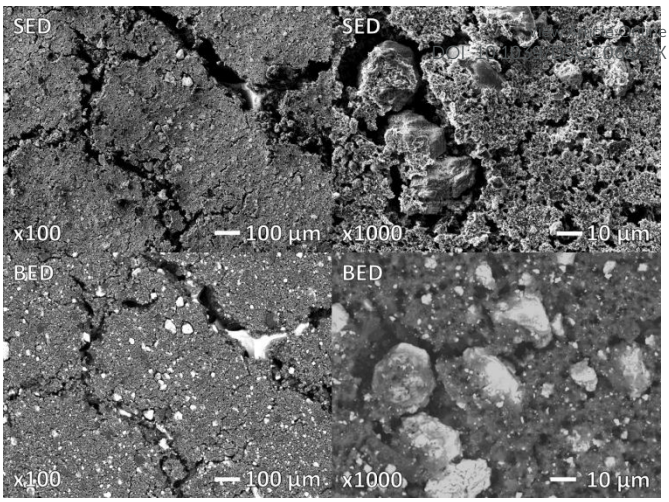

Figure 13. SEM after the application of 400 mA/cm^2 during experiments in Figure 11. This shows the limited effect of the experiments on the $NiCu_{0.2}$ containing electrode in comparison to **Error! Reference source not found.**. Both secondary electron detector (SED) and backscatter electron detector (BED) modes of SEM are applied to show topography and composition, respectively.

Potential corrosion structural changes and change in composition were determined using SEM and EDS. The used electrode (Figure 13) displayed macroscale cracking in comparison to the unused electrode (**Error! Reference source not found.**). However, the Ni current collector remains largely covered, with limited loss of $NiCu_{0.2}$ particles. BED modus confirms equivalent size and distribution of $NiCu_{0.2}$ material in the pristine and used electrodes. Additional particles were identified as $KOH \cdot 2H_2O$ and $KHCO_3$ salts in accordance with XRD. EDS analysis reported a composition of $NiCu_{0.04}$ for the electrode produced initially with $NiCu_{0.2}$ particles. Therefore, under the alkaline oxidative conditions from the experiments, a significant amount of Cu dissolved. Nonetheless, the remaining Cu concentration suggests resistance to further corrosion. Such Cu dissolution and corrosion could result in the copper complexes that are relatively stable, as indicated in Eq. 9-11.[43,44]

$$Cu^{2+} + 2\,OH^- \rightleftarrows CuO_{(s)} + H_2O \quad (9)$$

$$3\,Cu^{2+} + 4\,OH^- \rightleftarrows Cu_3(OH)_4^{2+} \quad (10)$$

$$3\,Cu^{2+} + 4\,OH^- \rightleftarrows Cu_3(OH)_4^{2+} \quad (11)$$

In forthcoming publication we will report on this $NiCu_{0.04}$ stable composition resulting after prolonged oxidation in 6 M KOH, and comparing to DFT calculations indicating its stability against dissolution as in Equation 9-11. However, here we note that even in the presence of ammonia and nitrite, $NiCu_{0.04}$ appears the remaining stable composition during prolonged experiments at industrial current densities.

Dual Product Electrolyser

This study demonstrated that it is possible to achieve high FE within 1 M NH_3 with selective conversion of ammonia to NO_2^-. This significant reduction in potential in comparison to OER, presents a possible method of reducing the potential of an electrolyser, while making a value-added product, rather than the oxygen waste product. However, this requires ammonia in the catholyte, which makes product purification more complex. The setup can be further optimized by balancing the K^+ transport through the CEM with flowing the catholyte into the anolyte (Figure 14). The nitrite could further be applied as fertilizer, while the H_2 could be used for energy storage or reinvested in the production of the consumed NH_3.

Overall, this system could be interesting for small scale synthetic fertilizer production, especially if local electricity is produced in excess due to intermittence. The end product could either be KNO_2 or NH_4NO_2, both are of value for contributing to the NPKS (nitrogen, phosphor, potassium, sulphur) ratio of synthetic fertilizer. With KOH balanced within the system, the only input is ammonia, water, and KOH to compensate product removal. The electrolyte could even be used directly, if the pH is balanced through the addition of phosphoric acid and sulfuric acid. The addition of these acids would contribute to the NPKS ratio of the fertilizer. Farmers would then be able to produce their own specific ratio with limited transport costs and shorter supply chains. Furthermore, this would limit the storing and transporting of ammonium nitrate, which is a potential hazardous substance.

View Article Online
DOI: 10.1039/D5GC06877K

ARTICLE

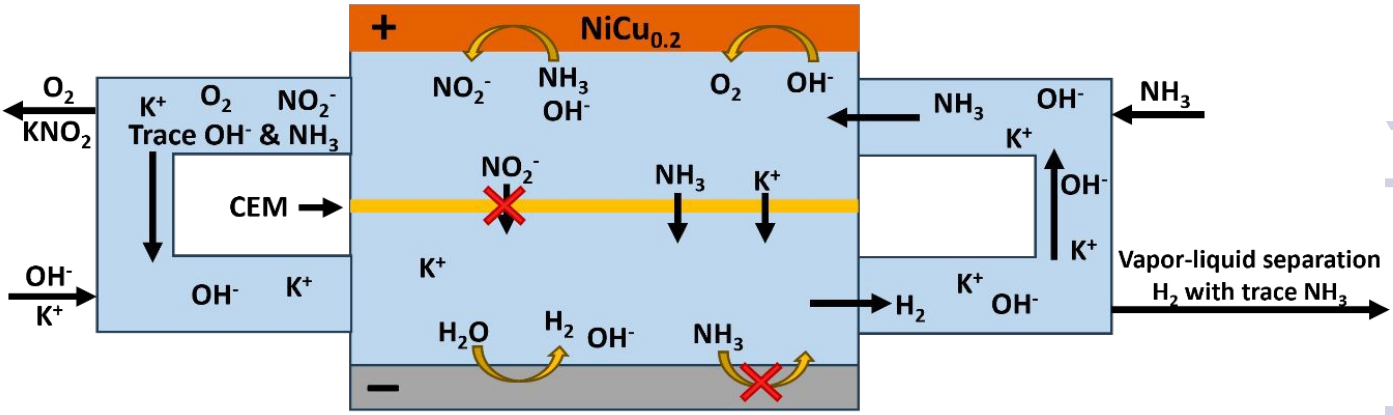

Figure 14. Schematic diagram of an AOR flow cell with central liquid flow, resulting in cycling of K^+ through the membrane. At the bottom negative electrode water reduction takes place, producing H_2 and OH^-. Charge compensating K^+ is transported through the CEM rather than protons under alkaline conditions. At the positive electrode, NH_3 oxidation to NO_2^- occurs using the OH^- (and trace water oxidation to O_2). The KOH and NH_3 input flow channels provide feeds to enable the overall reaction $KOH + H_2O + NH_3 \rightarrow KNO_2 + 3H_2$, as well as the (undesirable) OER. ammonium could be transported back into the bottom cell, if the pH permits its presence (e.g. at the outlet for KNO_2 where OH^- becomes depleted).

Conclusions

$Ni_{0.8}Cu_{0.2}(OH)_2$ has been investigated as a potential catalyst for ammonia oxidation to nitrite at industrially relevant current density and concentrations. The Cu was homogeneously incorporated within the β-$Ni(OH)_2$ phase to enhance the catalytic properties of $Ni(OH)_2$. The prepared $Ni_{0.8}Cu_{0.2}$ has a lower Tafel slope of 49 and 140 mV/dec at lower respectively higher current densities, compared to 62 and 186 mV/dec for the undoped $Ni(OH)_2$. In an undivided cell, the nitrite and nitrate yields are limited by the re-reduction of these products on the cathode. Furthermore, pH stabilisation with a supporting alkaline electrolyte is required to prevent pH reduction, which would also enable nitrite to nitrate oxidation.

In comparison, a Nafion® 117 cation exchange membrane divided cell under alkaline conditions results in consistent nitrite formation. This is only limited by ammonia depletion and by reduction of pH below 12. With this setup, the ammonia oxidation performance of $NiCu_{0.2}$ significantly improved with respect to yield and current densities. A faradaic efficiency towards nitrite of 67% at 2.5 mA/cm2 was achieved with 1 M ammonia in 6 M KOH. Furthermore, increasing the current density up to 400 mA/cm² improved the total faradaic efficiency to 96% with 95% NO_2^-:NO_3^- selectivity. This was achieved with 77% conversion in less than 3.5 hours. It was observed that the original $Ni_{0.83}Cu_{0.17}$ content was reduced in Cu content to $Ni_{0.96}Cu_{0.04}$ by the continuous ammonia oxidation. However, this composition is expected to remain stable, as it has also been observed in long term operation. The setup could be further optimised for synthetic fertilizer production, enabling small-scale fertilizer manufacturing. To conclude, we have successfully developed a copper-doped nickel hydroxide material that achieves promising results at industrial relevant current density and NH_3 concentration conditions. We suggest the application of a cation exchange membrane in future ammonia oxidation research to avoid skewing data towards N_2 formation.

Author contributions

Conceptualization: FM, DvN. Data acquisition and curation: DvN, PJ. Writing original draft: DvN, PJ, FM, Review and Editing: DvN, PJ,AU,FM, Funding acquisition: FM.

Conflicts of interest

There are no conflicts to declare.

Data availability

Data for this article are available at https://data.4tu.nl/datasets/eeb4617c-4c92-45d1-a0ab-57e41fb8889b/1

Acknowledgements

This research is funded by the Nitrogen Activation and Ammonia Oxidation project within the Electron to Chemical Bonds consortium with project number P17-08 which is financed by The Netherlands Organization for Scientific Research (NWO) and affiliated industrial partners.

References

[1], *Fertilizer Industry Handbook 2022*, YARA, **2022**.
[2], *Nitric Acid Market Size & Share Analysis - Growth Trends & Forecasts (2024 - 2029)*, Mordor Intelligence, **2024**.
[3] D. Chanda, R. Xing, T. Xu, Q. Liu, Y. Luo, S. Liu, R. Ashu Tufa, T. Heliso Dolla, T. Montini, X. Sun, "Electrochemical nitrogen reduction: recent progress and prospects" *Chemical Communications* **2021**, *57*, 7335–7349.
[4] Z. Huang, M. Rafiq, A. R. Woldu, Q.-X. Tong, D. Astruc, L. Hu, "Recent progress in electrocatalytic nitrogen reduction to ammonia (NRR)" *Coordination Chemistry Reviews* **2023**, *478*, 214981.
[5] X. Yang, S. Mukherjee, T. O'Carroll, Y. Hou, M. R. Singh, J. A. Gauthier, G. Wu, "Achievements, Challenges, and Perspectives on Nitrogen Electrochemistry for Carbon-Neutral Energy Technologies" *Angewandte Chemie* **2023**, *135*, e202215938.
[6] P. Jungbacker, R. Kortlever, F. M. Mulder, "Electrochemical nitrogen oxide formation from ammonia and dinitrogen" **n.d.**, DOI 10.1039/D5GC05480J.
[7] K. H. R. Rouwenhorst, F. Jardali, A. Bogaerts, L. Lefferts, "From the Birkeland–Eyde process towards energy-efficient plasma-based NOX synthesis: a techno-economic analysis" *Energy Environ. Sci.* **2021**, *14*, 2520–2534.
[8] M. Thiemann, E. Scheibler, K. W. Wiegand in *Ullmann's Encyclopedia of Industrial Chemistry*, John Wiley & Sons, Ltd, **2000**.
[9] W. Laue, M. Thiemann, E. Scheibler, K. W. Wiegand in *Ullmann's Encyclopedia of Industrial Chemistry*, John Wiley & Sons, Ltd, **2000**.
[10] K.-W. Kim, Y.-J. Kim, I.-T. Kim, G.-I. Park, E.-H. Lee, "Electrochemical conversion characteristics of ammonia to nitrogen" *Water Research* **2006**, *40*, 1431–1441.
[11] Y. Wang, Y. Yu, R. Jia, C. Zhang, B. Zhang, "Electrochemical synthesis of nitric acid from air and ammonia through waste utilization" *Natl Sci Rev* **2019**, *6*, 730–738.
[12] J. Cui, J. Hou, H. Pan, P. Kang, "Self-supporting CuM LDH (M = Ni, Fe, Co) carbon cloth electrodes for selective electrochemical ammonia oxidation to nitrogen" *Journal of Electroanalytical Chemistry* **2023**, *940*, 117502.
[13] M.-H. Tsai, T.-C. Chen, Y. Juang, L.-C. Hua, C. Huang, "High catalytic performance of CuCo/nickel foam electrode for ammonia electrooxidation" *Electrochemistry Communications* **2020**, *121*, 106875.
[14] G. Zhang, J. Ruan, T. Du, "Recent Advances on Photocatalytic and Electrochemical Oxidation for Ammonia Treatment from Water/Wastewater" *ACS EST Eng.* **2021**, *1*, 310–325.
[15] G. Jeerh, M. Zhang, S. Tao, "Recent progress in ammonia fuel cells and their potential applications" *Journal of Materials Chemistry A* **2021**, *9*, 727–752.
[16] Z.-H. Lyu, J. Fu, T. Tang, J. Zhang, J.-S. Hu, "Design of ammonia oxidation electrocatalysts for efficient direct ammonia fuel cells" *EnergyChem* **2023**, *5*, 100093.
[17] P. Zou, S. Chen, R. Lan, J. Humphreys, G. Jeerh, S. Tao, "Investigation of perovskite oxide SrFe0.8Cu0.1Nb0.1O3-δ as cathode for a room temperature direct ammonia fuel cell" *International Journal of Hydrogen Energy* **2019**, *44*, 26554–26564.
[18] Y. Huan, Y. He, S. Liu, Q. Cheng, F. Zhou, J. Wang, M. Wang, C. Yan, T. Qian, "Electrochemical Ammonia Oxidation Reaction on Nickel-Based Non-Noble Metal Electrocatalysts: From Mechanistic Understanding to Practical Applications" *Advanced Energy Materials* **2025**, *15*, e03815.
[19] S. Cohen, S. Johnston, C. K. Nguyen, T. D. Nguyen, D. A. Hoogeveen, D. V. Zeil, S. Giddey, A. N. Simonov, D. R. MacFarlane, "A CoOxHy/β-NiOOH electrocatalyst for robust ammonia oxidation to nitrite and nitrate" *Green Chem.* **2023**, *25*, 7157–7165.
[20] X. Jiang, D. Ying, X. Liu, M. Liu, S. Zhou, C. Guo, G. Zhao, Y. Wang, J. Jia, "Identification of the role of Cu site in Ni-Cu hydroxide for robust and high selective electrochemical ammonia oxidation to nitrite" *Electrochimica Acta* **2020**, *345*, 136157.
[21] S. Johnston, S. Cohen, C. K. Nguyen, K. N. Dinh, T. D. Nguyen, S. Giddey, C. Munnings, A. N. Simonov, D. R. MacFarlane, "A Survey of Catalytic Materials for Ammonia Electrooxidation to Nitrite and Nitrate" *ChemSusChem* **2022**, *15*, e202200614.
[22] S. Johnston, L. Kemp, B. Turay, A. N. Simonov, B. H. R. Suryanto, D. R. MacFarlane, "Copper-Catalyzed Electrosynthesis of Nitrite and Nitrate from Ammonia: Tuning the Selectivity via an Interplay Between Homogeneous and Heterogeneous Catalysis" *ChemSusChem* **2021**, *14*, 4793–4801.
[23] A. Kapałka, A. Cally, S. Neodo, C. Comninellis, M. Wächter, K. M. Udert, "Electrochemical

behavior of ammonia at Ni/Ni(OH)2 electrode" *Electrochemistry Communications* **2010**, *12*, 18–21.

[24] W. Xu, R. Lan, D. Du, J. Humphreys, M. Walker, Z. Wu, H. Wang, S. Tao, "Directly growing hierarchical nickel-copper hydroxide nanowires on carbon fibre cloth for efficient electrooxidation of ammonia" *Applied Catalysis B: Environmental* **2017**, *218*, 470–479.

[25] F. Almomani, M. Ali H Salah Saad, "Electrochemical oxidation of ammonia (NH4+/NH3) ON synthesized nickel-cobalt oxide catalyst" *International Journal of Hydrogen Energy* **2021**, *46*, 4678–4690.

[26] M. Zhu, Y. Yang, S. Xi, C. Diao, Z. Yu, W. S. V. Lee, J. Xue, "Deciphering NH3 Adsorption Kinetics in Ternary Ni–Cu–Fe Oxyhydroxide toward Efficient Ammonia Oxidation Reaction" *Small* **2021**, *17*, 2005616.

[27] A. Iranzo, F. M. Mulder, "Nickel-iron layered double hydroxides for an improved Ni/Fe hybrid battery-electrolyser" *Materials Advances* **2021**, *2*, 5076–5088.

[28] P.-P. R. M. L. Harks, C. B. Robledo, C. George, C. Wang, T. van Dijk, L. Sturkenboom, E. D. W. Roesink, F. M. Mulder, "Immersion precipitation route towards high performance thick and flexible electrodes for Li-ion batteries" *Journal of Power Sources* **2019**, *441*, 227200.

[29] P. Karanth, M. Weijers, P. Ombrini, D. Ripepi, F. Ooms, F. M. Mulder, "A phase inversion strategy for low-tortuosity and ultrahigh-mass-loading nickel-rich layered oxide electrodes" *CR-PHYS-SC* **2024**, *5*, DOI 10.1016/j.xcrp.2024.101972.

[30] B. Izelaar, D. Ripepi, D. D. van Noordenne, P. Jungbacker, R. Kortlever, F. M. Mulder, "Identification, Quantification, and Elimination of NOx and NH3 Impurities for Aqueous and Li-Mediated Nitrogen Reduction Experiments" *ACS Energy Lett.* **2023**, *8*, 3614–3620.

[31] N. I. Watson, M. Keegan, B. van den Bosch, N. Yan, G. Rothenberg, "The Influence of Metal Impurities on NiOOH Electrocatalytic Activity in the Oxygen Evolution Reaction" *ChemElectroChem* **2024**, *11*, e202400223.

[32] M. A. Ahsan, A. R. Puente Santiago, Y. Hong, N. Zhang, M. Cano, E. Rodriguez-Castellon, L. Echegoyen, S. T. Sreenivasan, J. C. Noveron, "Tuning of Trifunctional NiCu Bimetallic Nanoparticles Confined in a Porous Carbon Network with Surface Composition and Local Structural Distortions for the Electrocatalytic Oxygen Reduction, Oxygen and Hydrogen Evolution Reactions" *J. Am. Chem. Soc.* **2020**, *142*, 14688–14701.

[33] W. Xu, D. Du, R. Lan, J. Humphreys, D. N. Miller, M. Walker, Z. Wu, J. T. S. Irvine, S. Tao, "Electrodeposited NiCu bimetal on carbon paper as stable non-noble anode for efficient electrooxidation of ammonia" *Applied Catalysis B: Environmental* **2018**, *237*, 1101–1109.

[34] M.-H. Tsai, Y. Juang, C.-C. Hu, L.-C. Hua, B. K. Mahata, C. Huang, "The direct electrocatalytic oxidation of ammonia by copper-deposited nickel foam catalysts" *Electrochimica Acta* **2023**, *446*, 142130.

[35] M. Zhang, J. Zhang, G. Jeerh, P. Zou, B. Sun, M. Walker, K. Xie, S. Tao, "A symmetric direct ammonia fuel cell using ternary NiCuFe alloy embedded in a carbon network as electrodes" *J. Mater. Chem. A* **2022**, *10*, 18701–18713.

[36] E. Latvytė, X. Zhu, L. Wu, R. Lan, P. Vale, J. E. Graves, "A low-temperature ammonia electrolyser for wastewater treatment and hydrogen production" *International Journal of Hydrogen Energy* **2024**, *52*, 265–282.

[37] D. Ripepi, B. Izelaar, D. D. van Noordenne, P. Jungbacker, M. Kolen, P. Karanth, D. Cruz, P. Zeller, V. Pérez-Dieste, I. J. Villar-Garcia, W. A. Smith, F. M. Mulder, "In Situ Study of Hydrogen Permeable Electrodes for Electrolytic Ammonia Synthesis Using Near Ambient Pressure XPS" *ACS Catalysis* **2022**, *12*, 13781–13791.

[38] J. J. Medvedev, Y. Tobolovskaya, X. V. Medvedeva, S. W. Tatarchuk, F. Li, A. Klinkova, "Pathways of ammonia electrooxidation on nickel hydroxide anodes and an alternative route towards recycled fertilizers" *Green Chem.* **2022**, *24*, 1578–1589.

[39] G. Cacciola, G. Restuccia, Yu. Aristov, "Vapor Pressure of (Potassium Hydroxide + Ammonia + Water) Solutions" *J. Chem. Eng. Data* **1995**, *40*, 267–270.

[40] R. Barnard, C. F. Randell, F. L. Tye, "Studies concerning charged nickel hydroxide electrodes I. Measurement of reversible potentials" *J Appl Electrochem* **1980**, *10*, 109–125.

[41] V. Srinivasan, J. W. Weidner, R. E. White, "Mathematical models of the nickel hydroxide active material" *J Solid State Electrochem* **2000**, *4*, 367–382.

[42] X. Xie, L. Du, L. Yan, S. Park, Y. Qiu, J. Sokolowski, W. Wang, Y. Shao, "Oxygen Evolution Reaction in Alkaline Environment: Material Challenges and Solutions" *Advanced Functional Materials* **2022**, *32*, 2110036.

View Article Online
DOI: 10.1039/D5GC06877K

[43] X. Wang, Q. Chen, H. Hu, Z. Yin, Z. Xiao, "Solubility prediction of malachite in aqueous ammoniacal ammonium chloride solutions at 25 °C" *Hydrometallurgy* **2009**, *99*, 231–237.
[44] I. Puigdomenech, C. Taxén, *Thermodynamic data for copper*, Svensk Kärnbränslehantering AB, **2000**.

View Article Online
DOI: 10.1039/D5GC06877K

Data Availability statement of

Data for this article are available at
https://data.4tu.nl/datasets/eeb4617c-4c92-45d1-a0ab-57e41fb8889b/1